Biogeosciences Discuss., 6, 11317–11345, 2009
www.biogeosciences-discuss.net/6/11317/2009/

Biogeosciences Discussions

This discussion paper is/has been under review for the journal Biogeosciences (BG).
Please refer to the corresponding final paper in BG if available.

Upscaling of gross ecosystem production to the landscape scale using multi-temporal Landsat images, eddy covariance measurements and a footprint model

B. Chen[1,2], Q. Ge[1], D. Fu[1], G. Liu[1], G. Yu[1], X. Sun[1], S. Wang[1], and H. Wang[1]

[1]LREIS Institute of Geographic Sciences and Nature Resources Research, Chinese Academy of Sciences, Beijing 100101, China
[2]Department of Forest Resources Management, Faculty of Forestry, University of British Columbia, 2424 Main Mall, Vancouver, BC, V6T 1Z4, Canada

Received: 3 September 2009 – Accepted: 16 November 2009 – Published: 1 December 2009

Correspondence to: B. Chen (baozhang.chen@igsnrr.ac.cn)

Published by Copernicus Publications on behalf of the European Geosciences Union.

Abstract

In order to use the global available eddy-covariance (EC) flux dataset and remote sensing measurements to provide estimates of gross primary production (GPP) at landscape (10^1–10^2 km^2), regional (10^3–10^6 km^2) and global land surface scales, we developed a satellite-based GPP algorithm using Landsat data and an upscaling framework. The satellite-based GPP algorithm uses two improved vegetation indices (Enhanced Vegetation Index – EVI, Land Surface Water Index – LSWI). The upscalling framework involves flux footprint climatology modeling and data-model fusion. This approach was first applied to an evergreen coniferous stand in South China subtropical monsoon climatic zone. The EC measurements at Qian Yinzhou tower site (26° 44′ 48″ N, 115° 04′ 13″ E), which belongs to the Chinaflux network, and the Landsat images for this region in 2004 were used in this study. The seasonal dynamics of GPP predicted by the satellite-based algorithm agreed well with observed GPP in 2004 at this site. These results demonstrate the potential of combining of the satellite-based algorithm, flux footprint modeling and data-fusion, for scaling-up of GPP at the CO_2 flux tower sites, a key component for the study of the carbon cycle at regional and global scales.

1 Introduction

Growing interest in climate change has stimulated recent research that aims to quantify components of the natural carbon (C) cycle. The eddy-covariance technique (EC) is commonly used to directly measure the CO_2, water vapor and energy exchange between the atmosphere and terrestrial ecosystems (Baldocchi, 2008). Today, there exist more than 400 EC-flux towers across continents. EC measurements are a rich source of information on temporal variability and environmental controls of CO_2 exchange between the atmosphere and terrestrial ecosystems (Law et al., 2000). These global EC datasets provide investigators opportunities and information to 1) explore emergent-scale properties by quantifying how the metabolism of complex ecosystems respond

BGD

6, 11317–11345, 2009

to perturbations in climate variables on diurnal, seasonal, interannual and decadal time scales and elucidate physical and biological controlling factors (Law et al., 2000; Baldocchi, 2008); 2) examine carry-over effects that may be introduced by either favorable or deleterious conditions during antecedent years (Barford et al., 2001); 3) observe a disturbance and the recovery from it or to span a natural sequence of ecological development coupled with fluctuations in climate (Amiro et al., 2006; Stoy et al., 2006); and 4) test and validate ecosystem process models (Chen et al., 2007; Urbanski et al., 2007), since most of these models span timescales from hours to decades. Although the available EC data have been rapidly accumulating, much of this information is of limited use because of the difficulties/uncertainties in i) assessing/interpreting the associated measuring biases of EC data and ii) upscaling of the EC fluxes at the ecosystem (typically less than 1–3 km^2 for each site) to larger scales, e.g. landscape and regional scales.

The EC method is based on measurements of turbulent fluctuations of the vertical velocity and the concentration of a passive tracer. Knowledge of the area's soil and vegetation that impacts the EC flux is clearly important both in planning the site tower location and in the interpretation of measured fluxes (Finnigan, 2004). The adoption of the EC technique to estimate surface exchange is based on the assumption that certain meteorological conditions (e.g. horizontal homogeneity, steady-state, and non-advection) are satisfied (Göckede et al., 2004). Since such conditions are often violated in complex terrain, e.g. at flux monitoring sites in forests, correct interpretation of EC-data is still a matter of some difficulty (Sogachev et al., 2004). In particular, the spatial variability of vegetation density influences the lower atmospheric circulation and surface exchange of energy, water and C over a wide range of scales (e.g., Shen and Leclerc, 1995; Buermann et al., 2001; Cosh and Brutsaert, 2003). As a result, evaluation of the spatial representativeness of long-term accumulated EC-flux measurements is still challenging (Chen et al., 2009a).

Footprint analysis is a recognized part of the establishment and siting of flux towers and the analysis of their output (Finnigan, 2004). The interpretation of EC flux

measurements over a heterogeneous surface depends largely on the footprint over which the fluxes are sampled. The temporal and spatial variability of footprints and the associated influence of varying site heterogeneities on tower flux measurements has yet to be fully been investigated, although this information is critical needed for interpretation and for making a more wide use of the globally available EC datasets which have been rapidly accumulating.

In order to use EC flux measurements to provide estimates of components of the natural C cycles at landscape (10^1–10^2 km^2), regional (10^3–10^6 km^2), or hemispheric to global land surface (10^7–10^8 km^2) scales, they must be reasonably "upscaled" using either models and/or remote sensing measurements (e.g. Earth observation (EO) data). However, it has been proved that, it is an extremely challenging task to scale up those EC measurements from stand-level to a region or global scales because of the large spatial heterogeneity and temporal dynamics of ecosystems across complex landscapes and regions and the nonlinearity inherent in ecophysiological processes (Levy et al., 1999; Chen et al., 2007; Hilker et al., 2008).

Satellite remote sensing can provide consistent and systematic observations of vegetation and ecosystems over large spatial extents on variable spatial and temporal resolutions. For example, the Moderate Resolution Imaging Spectroradiometer (MODIS) is a 36 band spectrometer providing a global data set every 1–2 d. The spatial resolution of MODIS (pixel size at nadir) is 250 m for channel 1 and 2 (0.6–0.9 μm), 500 m for channel 3 to 7 (0.4–2.1 μm) and 1000 m for channel 8 to 36 (0.4–14.4 μm), respectively. The Landsat Enhanced Thematic Mapper Plus (ETM+) is a sensor carried onboard the Landsat 7 satellite and has acquired images of the Earth at 30 m spatial resolution with a 16-d repeat cycle. Data from the satellite-borne MODIS are currently used in the calculation of global weekly gross primary productivity (GPP) at 1-km spatial resolution (Running et al., 2004; Coops et al., 2007). These data with variable spatial and temporal resolutions, however, require appropriate methods for upscaling and interfacing EC-measurements to satellite observations (Drolet et al., 2008; Hall et al., 2008). It is challenging to compare the estimated GPP using MODIS satellite

BGD
6, 11317–11345, 2009

data at 1-km resolution with the EC-derived GPP because of mismatch between them in spatial scales (Xiao et al., 2004). Whereas, the Landsat imagines have fine resolutions (i.e. 30 m), which are ideal for spatial scaling and comparison of C fluxes derived from satellite-borne and EC data with assistance of flux footprint analysis (Chen et al., 2009a).

The objective of this study is twofold: 1) to examine biophysical performance of vegetation indices in relation to seasonal dynamics of CO_2 fluxes; and 2) to develop a practical approach for upscaling GPP to the landscape scale and assessing the EC sensor location biases (i.e. the influence of patch-scale heterogeneities and the spatial representativeness of the EC flux footprint on the uncertainty in EC CO_2 flux data) using the Landsat images and a recently developed footprint model (Chen et al., 2009a). Qian Yanzhou (QYZ) EC flux tower site, locating in South China subtropical monsoon climatic zone at 26° 44′ 48″ N, 115° 04′ 13″ E, which belongs to the Chinaflux network, was selected as an experiment site. The EC data measured at this tower and the Landsat images in 2004 were used in this study. Firstly, footprint climatology across multi-temporal scales (i.e. daily, biweekly, monthly and annual) was calculated using the Simple Analytical Footprint model on Eulerian coordinates (SAFE, Chen et al., 2008, 2009a); secondly, biweekly high-spatial-resolution GPP maps were produced based on the Landsat data using a light-use efficiency modeling approach (e.g., Xiao et al., 2004); and finally these year-round estimates of GPP were compared to that directly derived from EC measurements using two alternative weighting approaches, i.e. footprint weighting or "equal" weighting. These comparisons provided opportunities to optimize the parameters used in the light-use efficiency model and to estimate the tower sensor location biases caused by the variations in size and orientation of footprint climatology and patch-scale heterogeneities.

2 Materials and methods

2.1 Site description

The study site, QYZ Experimental Station, which belongs to Chinese Ecosystem Research Network (CERN) and ChinaFLUX network, is located in southeastern China (elevation 102 m). The mean annual air temperature was 17.9°C, and mean annual precipitation was 1485 mm (1985–2004). Most areas in the same latitude zone as QYZ around the world are arid steppes or deserts. The warm and humid environment in QYZ is the result of unique southeast monsoon. QYZ is located on gently undulating terrain with slopes between 2.88 and 13.58 (Wen et al., 2006). The QYZ ecological experimental station was established in 1983, at that time the area was mainly covered by wild grasslands, shrub lands and some sparse *Pinus massoniana*. After the experimental station setup, the land covers of QYZ were changed much by scientists (Huang et al., 2007). The EC flux tower was established in late August of 2002. The dominated trees in the flux footprint area are *Pinus elliottii*, *Pinus massoniana* and *Cunninghamia lanceolata*. The stand characteristics at QYZ based on a survey made in 2005 (Wen et al., 2006) are list in Table 1. According to the field measurements in August of 2003, the leaf area index (LAI) of the plantation was 4.5 (Huang et al., 2007). The understory shrub mainly includes *Loropetalum Chinense* and *Lyonia compta*. The soil is red soil, which weathered from red sand rock.

2.2 EC flux and meteorological measurements

CO_2, water vapour and energy exchange, and meteorological variables were measured continuously at the QYZ site from 2003. Measurements, instruments, calculation procedures and gap filling methodologies were described in Wen et al. (2006). Net ecosystem exchange (NEE) was calculated as the sum of the EC CO_2 flux above the canopy and the change in CO_2 storage in the air column between the EC-sensor height and the ground (Wen et al., 2006). Ecosystem respiration (R_{eco}) at night was assumed

to equal NEE in well-mixed conditions, i.e., friction velocity (u_*) larger than a threshold value (u_*^{th}=0.2 m s^{-1}). Daytime R_{eco} and values to fill nighttime gaps were calculated using the relationship between nighttime NEE in well-mixed conditions and soil temperature at the 5-cm depth (Wen et al., 2006). Net ecosystem productivity (NEP) was calculated as NEP=−NEE. GPP was calculated as the sum of daytime NEP and calculated daytime R_{eco}.

2.3 Data-model fusion and upscaling framework based on Landsat images

An algorithm for estimating landscape and regional C fluxes (e.g. GPP) includes the following four steps (Fig. 1): i) A satellite-based vegetation photosynthesis model was adopted to produce GPP maps at 30 m resolutions using Landsat and climate data; ii) EC flux footprints for the corresponding Landsat repeating periods (normally bi-weekly) were calculated using a recently developed footprint model (SAFE, Chen et al., 2009a); iii) By assuming the footprint integration of remotely-sensed GPP to be comparable with the EC-derived GPP values, several key parameters in the satellite-based vegetation photosynthesis model were optimized using the data-model fusion technique; and iv) The updated satellite-based vegetation photosynthesis model was used for data fusion with other satellite data (e.g. MODIS) or directly used for estimating landscape/regional GPP.

2.4 An algorithm for estimating GPP based on Landsat data

2.4.1 Overview of the algorithm

Satellite-based studies have used the light-use efficiency (ε) approach to estimating GPP (Prince and Goward, 1995; Running et al., 2000, 2004; Behrenfeld et al., 2001) or net primary production (NPP) (Field et al., 1995; Ruimy et al., 1999). Significant effort and progress have been made in developing the satellite-based GPP algorithms (Running et al., 2004; Xiao et al., 2004, 2005). Similar to the MODIS GPP algorithm

(Running et al., 2004) and the vegetation photosynthesis model (Xiao et al., 2004), the algorithm (Fig. 2) used in this study relies on the light-use efficiency (ε) approach relating GPP to the amount of absorbed photosynthetically active radiation (APAR) (Monteith, 1966, 1972) such that,

$$\mathrm{GPP} = \varepsilon \times f\mathrm{PAR}_{\mathrm{chl}} \times \mathrm{PAR}, \quad (1)$$

where PAR is the photosynetically active radiation (in μmol photosynthetic photon flux density, PPFD), $f\mathrm{PAR}_{\mathrm{chl}}$ is the fraction of PAR absorbed by leaf chlorophyll in the canopy, and ε is the light use efficiency (μmol CO_2/μmol PPFD). Light use efficiency (ε) is affected by leaf phenology, temperature, and water:

$$\varepsilon = \varepsilon_0 \times P_{\mathrm{m}} \times W_{\mathrm{m}} \times T_{\mathrm{m}}, \quad (2)$$

where ε_0 is the apparent quantum yield or maximum light use efficiency (μmol CO_2/μmol PPFD) for a given land cover type or vegetation function type, and P_{m}, W_{m} and T_{m} are the modifiers for the effects of leaf phenology, water and temperature on light use efficiency of vegetation, respectively.

2.4.2 Model parameter estimates

Different parameters and inputs for the satellite-based algorithm are estimated in different ways: i) the fraction of PAR absorbed by leaf chlorophyll in the canopy ($f\mathrm{PAR}_{\mathrm{chl}}$) and the modifiers ($P_{\mathrm{m}}$, W_{m}) are estimated using Landsat imagery data; ii) PAR and temperature modifier (T_{m}) are calculated using climate data (either from tower measurements or climate models); and iii) the maximum light use efficiency (ε_0) is referred to the land-cover-related look-up table and then modified/optimized using EC tower C measurements and footprint climatology.

To accurately estimate $f\mathrm{PAR}_{\mathrm{chl}}$ in forests is a challenge to both radiative transfer modeling and field measurements. Significant effort and progress have been made in developing advanced vegetation indices that are optimized for retrieval of fPAR from individual optical sensors (Gobron et al., 1999; Govaerts et al., 1999). In this study, the

BGD
6, 11317–11345, 2009

fPAR within the photosynthetically active period of vegetation is estimated as a linear function of the Enhanced Vegetation Index (EVI),

$$f\mathrm{PAR} = \mathrm{EVI}, \tag{3}$$

where EVI directly normalizes the reflectance in the red band as a function of the reflectance in the blue band (Huete et al., 1997):

$$\mathrm{EVI} = G \times (\rho_{\mathrm{nir}} - \rho_{\mathrm{red}}) / (\rho_{\mathrm{nir}} + C_1 \times \rho_{\mathrm{red}} - C_2 \times \rho_{\mathrm{blue}} + L) \tag{4}$$

where G=2.5, C_1=6, C_2=7.5, and L=1 (Huete et al., 1997); and ρ_{nir}, ρ_{red} and ρ_{blue} are the reflectance of near infrared bands, red bands and blue bands, respectively.

The leaf phenology modifier (P_{m}) is estimated using the Normalized Difference Vegetation Index (NDVI) and the Land Surface Water Index (LSWI). NDVI (Tucker, 1979; Field et al., 1995) and LSWI (Xiao et al., 2002) are calculated, respectively using Eqs. (5) and (6):

$$\mathrm{NDVI} = (\rho_{\mathrm{nir}} - \rho_{\mathrm{red}}) / (\rho_{\mathrm{nir}} + \rho_{\mathrm{red}}), \tag{5}$$

$$\mathrm{LSWI} = (\rho_{\mathrm{nir}} - \rho_{\mathrm{swir}}) / (\rho_{\mathrm{nir}} + \rho_{\mathrm{swir}}), \tag{6}$$

where ρ_{nir}, ρ_{red} and ρ_{swir} are the reflectance of near infrared bands, red bands and short infrared bands, respectively. P_{m} is calculated at two different phases, depending upon life expectancy of leaves (deciduous versus evergreen):

$$P_{\mathrm{m}} = \begin{cases} \frac{1+\mathrm{LSWI}}{2} & \text{During bud burst to leaf full expansion} \\ 1 & \text{After leaf full expansion} \end{cases} \tag{7}$$

The timings of bud burst and leaf full expansion can be identified using NDVI. The effect of water on plant photosynthesis (W_m) has been estimated as a function of available soil content in plant root zone and water vapor pressure deficit (VPD) in a number of process-based ecosystem models (e.g., Chen et al., 2007) and remote-sensing based models (e.g., Running et al., 2000). Soil moisture represents water supply to the leaves

and canopy, and VPD represents evaporative demand in the atmosphere. Leaf and canopy water content is largely determined by the dynamics of both soil moisture and VPD. As the first order of approximation, here following the alternative and simple approach that uses a satellite-derived water index (Xiao et al., 2004), we use Eq. (8) to estimate the seasonal dynamics of W_m:

$$W_m = (1 + \mathrm{LSWI})/(1 + \mathrm{LSWI}_{\max}), \tag{8}$$

where $\mathrm{LSWI}_{\max}$ is the maximum LSWI within the plant growing season for individual pixels. The temperature modifier T_m was estimated at each time step, using the equation developed for the terrestrial ecosystem model (Raich et al., 1991):

$$T_\mathrm{m} = \frac{(T - T_{\min})(T - T_{\max})}{[(T - T_{\min})(T - T_{\max})] - (T - T_{\mathrm{opt}})^2} \tag{9}$$

where $T_{\min}$, $T_{\max}$ and T_{opt} are the minimum, maximum and optimal temperature for photosynthetic activities, respectively. Their values are respectively set to be 0, 35 and 20°C in this study. If air temperature falls below $T_{\min}$, T_m is set to be zero.

The ε_0 values vary with vegetation types, and the information about ε_0 for individual vegetation types can be obtained from a survey of the literature (Ruimy et al., 1995) and optimized using EC tower measurements. According to the work (Zhang et al., 2006), the ε_0 value was estimated to be 0.032 μmol CO_2/μmol PPFD in this study stand in 2004.

2.5 Footprint and footprint climatology estimates

We use the Simple Analytical Footprint model on Eulerian coordinates (SAFE, Chen et al., 2008, 2009a) to calculate QYZ EC tower's footprints. The flux footprints were calculated at a grid size of 30 m×30 m (consistent with the Landsat spatial resolutions) covering the area (domain) centred on the towers of 6 km×6 km. The model was run at half-hourly time steps. The half-hourly footprint $f(x,y)$ was rotated along the wind

direction and cumulated to biweekly, monthly and annual time steps to yield the information on footprint climatology, $\phi(x,y)$. The total footprint $\Phi = \iint_{\Omega_\Pi} \phi dxdy$ within the model domain (Ω_Π) equals 1. The calculated footprint provides a map of the contribution for the area around the tower to the integral EC-measured flux component. The detailed description of footprint model and the footprint climatology calculations can been found in Chen et al. (2009a).

2.6 Scaling of remotely sensed GPP to EC-flux derived GPP

The ecosystem-scale overall GPP ($F_{GPP,rs}$) was up-scaled from the spatial distributed GPP field ($F_{GPP,rs}$) using Eq. (10),

$$F_{GPP,\phi} = \iint_{\Omega_\Pi} F_{GPP,rs}(x,y)\phi_{pure}(x,y)dxdy. \quad (10)$$

In Eq. (10), ϕ_{pure} is the pure footprint and Ω_Π is the upwind footprint source area. Both $F_{GPP,rs}$ and ϕ_{pure} were estimated at 30-m resolution. The EC-derived GPP value is expected to be close to the value of $F_{GPP,rs}$ weighted with ϕ_{pure} over Ω_Π. "Equal" integration of $F_{GPP,rs}$ was also calculated using Eq. (10) by setting ϕ_{pure} to be 1 over Ω_Π. Both footprint integration and "Equal" integration of $F_{GPP,rs}$ were calculated at biweekly time steps first and then summed up to gain annual values for comparisons. Comparisons of ecosystem-scale GPP estimates between integrated from $F_{GPP,rs}$ and directly derived from EC measurements were made for the year of 2004 at the QYZ site.

2.7 Sensor location bias

The spatial representativeness of the footprint is given by the sensor location bias (Δ) following Schmid (1997),

$$\Delta = (F_{GPP,\phi} - F_{GPP,\phi=1})^2 / (F_{GPP,\phi=1})^2, \quad (11)$$

where $F_{GPP,\phi}$ and $F_{GPP,\phi=1}$ is the footprint-weighted and "equally"-weighted GPP, respectively. Alternatively, the sensor location bias was also estimated by replacing the "equally" integrated $F_{GPP,\phi=1}$ with the GPP values of the tower location pixel. The values of Δ and of root bias δ ($\delta = \sqrt{\Delta}$) were calculated at biweekly time steps and then averaged to gain monthly and annual values for the year of 2004 at QYZ.

2.8 Dataset used

The Landsat image data in 2004 for the area (domain) of 6 km×6 km centered at the QYZ tower acquired from the website of US Geological Survey at http://glovis.usgs.gov/. The NDVI (Fig. 3), EVI and LSWI were calculated based on the Landsat original data after atmospheric and other corrections. The QYZ tower data in 2004 were used for footprint calculations and several key parameters (e.g. ε_0) of the satellite-based GPP algorithm estimates and for GPP comparisons. The seasonal dynamics of C flux components measured at QYZ in 2004 were shown in Fig. 4.

3 Results

3.1 Variations in seasonal footprint climatology

Figure 5 shows the mean monthly daytime pure footprints and the corresponding cumulative footprint contours for every other months in 2004 for QYZ. The seasonal variations in size and orientation of footprint for QYZ are significant. The areas of 90% cumulative footprints in winter months were less than 1 km^2 whist were as large as 2.5 km^2 in summer months.

3.2 Comparing estimated values of remotely sensed and EC derived GPP

The remotely-sensed biweekly mean GPP maps at 30 m resolution were produced based on Landsat image data, which overlaid by the corresponding period daytime

footprint. Figure 6 shows an example at annual time step. The spatial variations of remotely-sensed GPP were not obvious for this plantation stand. The elliptical shape of the annual footprint distributed along the NNW-SSE prevailing wind directions. The size of the annual mean 90% cumulative footprint was about 1.5 km^2.

The ecosystem-scale overall biweekly GPP (namely footprint-integrated GPP) was up-scaled from these spatially distributed GPP field using Eq. (10). The "equally" integrated GPP was also calculated using Eq. (10) by setting $\phi_{pure}=1$ for comparisons. The remotely-sensed GPP using Landsat data reasonably followed the seasonal dynamics of observed GPP (Figs. 7 and 8). During winter time (when GPP<=~3 g m^{-2} d^{-1}), the remote-sensing algorithm underestimated the measured GPP; while during summer time (when GPP>=~7 g m^{-2} d^{-1}), the remote-sensing algorithm overestimated the observed GPP (Figs. 7 and 8). The footprint integrated GPP values were closer to EC-derived GPP values than the "equally" integrated GPP and the tower pixel's GPP values though their differences were small. The annual mean GPP values were 5.15, 5.06, 4.51 and 5.09 g C m^{-2} s^{-1} for EC-derived, footprint-integrated, "equally"-integrated and the tower pixel's GPP, respectively. As shown in Figs. 3 and 6, the land surface heterogeneity is quite small for this plantation stand, therefore the annual mean tower location biases was less than 5%. Even for this "ideal" EC tower location, the estimated biases in annual sum of GPP at the landscape scale between with or without footprint consideration could be as large as 200 g C m^{-2}.

4 Discussion

The seasonal phenologically dynamics of canopy development (leaf flush, expansion, senescence, fall), in relation to their biophysical, biochemical (e.g., chlorophyll and other pigments, nitrogen) and optical properties, which in turn influence both biophysical parameters (e.g., albedo, latent and sensible heat fluxes) and biogeochemical parameters (e.g., photosynthesis) of the land surface (Xiao et al., 2004; Li et al., 2007). Therefore, the time series of the vegetation indices have potential to provide valuable

insight into the processes (e.g., growing season length and water condition) that regulate ecosystem carbon exchange. NDVI and EVI are widely applied to detect the information on leaf area index (Chen et al., 2006) and *f*PAR (Running et al., 2004; Xiao et al., 2004). A number of studies demonstrated that the seasonal dynamics of MODIS EVI agreed better with GPP than MODIS NDVI for different ecosystems (e.g. evergreen needleleaf forest, Xiao et al., 2004; alpine ecosystems in Qinghai-Tibetan Plateau, Li et al., 2007). The availability of time-series data of SWIR and NIR bands from the new generation of optical sensors (e.g., VGT, MODIS, Landsat 7) offer new opportunity for quantifying canopy water content at large spatial scales (Xiao et al., 2004). These sensor-specific advanced vegetation indices (e.g. EVI and LSWI) have been optimized for the Moderate Resolution Imaging Spectroradiometer (MODIS), the Global Imager (GLI) and the VEGETATION sensors (Li et al., 2007). Clearly, there is a need to examine those advanced vegetation indices for all available satellite sensors in relation to leaf phenology and the seasonal dynamics of GPP across the flux tower sites in various biomes. Limited number of studies had evaluated radiometric and biophysical performance of vegetation indices (e.g. EVI, NDVI) from Landsat data, probably because of mismatch of spatial resolutions between Landsat data and EC flux towers.

The performance of a new algorithm based on the advanced vegetation indices using Landsat data was evaluated with assistance of a footprint model. A good agreement between predicted and EC measured biweekly GPP in 2004 in an evergreen needleleaf forest at QYZ (R^2=0.9, p<0.001, Fig. 8) indicates that there exist a good quantitative relationship between the Landsat vegetation indices and CO_2 flux data, in terms of the seasonal phase and magnitude of photosynthesis. However, the discrepancies between remotely-sensed and EC-derived GPP are still large, especially in winter and in the middle of summer (Fig. 7). Those large discrepancies may be attributed to three sources of errors. The first source is the sensitivity of the remote sensing algorithm to PAR and T_m. The parameters for estimating T_m in Eq. (9), T_{min}, T_{max} and T_{opt} are vegetation-type and climate-zone dependent, and may vary with different seasonal

phases. In this study, we simply assume those parameters have no seasonal variations. This may lead to ill parameterization of T_m, such as over-corrected (smaller values of T_m) during the low-temperature periods while under-corrected (larger values of T_m) during the high-temperature periods. The second source is the time-series data of vegetation indices from Landsat satellite images. We used the biweekly Landsat data that have no BRDF correction or normalization, and thus, the effect of angular geometry on surface reflectance and vegetation indices remained. EVI is a semi-empirical mathematic transformation of observed reflectance from individual spectral bands (blue, red and NIR) of optical sensors (Huete et al., 2002). The parameters in Eq. (4) may vary seasonally. For simplification, however, we only optimized one value for each parameter and applied it to the whole year period. The third source is the error in EC-derived GPP. The EC measurements themselves are not free from error. The partitioning of NEE into its component fluxes (i.e. GPP and R_{eco}) has large uncertainties (Falge et al., 2001; Chen et al., 2009b). The two major steps to derive GPP are the gap filling of NEE and estimation of daytime ecosystem respiration, and both of them carried on a lot of uncertainties.

The maximum light use efficiency (ε_0) is the basis for the remote-sensing based algorithms or models and the accurate estimating of ε_0 is one of the key steps for using the satellite data to estimate either GPP or NPP (Running et al., 1999). In nature, ε_0 is determined by many biological and biophysical factors and soil nutrient conditions. Much attention should be given to the variability of ε_0 among vegetation types across a heterogeneous landscape (Li et al., 2007). Since ε_0 differs significantly among vegetation types, these differences should be accounted for when estimating GPP using remotely-sensed data. These global EC datasets provide investigators opportunities to estimate the ecosystem-scale photosynthetic (including ε_0) and respiratory parameters. A widely-used method for those parameters estimation is the Michaelis-Menten approach (Falge et al., 2001). Caution should be paid when we apply the EC-derived ε_0 to remote-sensing-based algorithms for GPP estimates because: i) there are large uncertainties in the EC-derived ε_0; ii) the values of EC-derived ε_0 vary seasonally and

BGD
6, 11317–11345, 2009

interannually; and iii) the EC-derived ε_0 represents the EC flux footprint area, whose sizes and orientations vary with time, in other words, the spatial representativeness of the EC-derived ε_0 is normally different from the satellite image pixels. Making use of the satellite data with fine resolution (e.g. Landsat data) to estimate GPP, flux footprint modeling should be involved to optimize the remote-sensing-based algorithms' parameters, such as ε_0, T_m etc. These optimized parameters then can transfer to the applications of other satellite images with coarse resolution (e.g. MODIS) by applying data-fusion techniques. Combining vegetation indices (e.g. EVI, LSWI) from different multi-temporal/spatial satellite sensors' data, climate data (PAR, temperature), optimized ε_0 parameter for individual vegetation types, and flux footprint modeling and data-fusion, the remote-sensing-based algorithms is a powerful tool for estimating landscape/regional or global GPP.

Acknowledgements. This research is financially supported by "One hundred talents" program funded by Chinese Academy of Sciences, National Key Technology R&D Program of China (2008BAK50B06-02), and Alexander Graham Bell Canada Scholarship (CGS) funded by Natural Sciences and Engineering Research Council of Canada. We gratefully thank Dr. N. C. Coops (UBC) for his valuable scientific input. We thank W. Zhang (IGSNRR) for providing the Qian Yizhou flux tower data.

References

Amiro, B. D., Barr, A. G., and Black, T. A.: Carbon, energy and water fluxes at mature disturbed forest sites, Saskatchewan, Canada, Agr. Forest Meteorol., 136, 237–251, 2006.

Baldocchi, D. D.: Breathing of the terrestrial biosphere: lessons learned from a global network of carbon dioxide flux measurement systems, Aust. J. Bot., 56, 1–26, 2008.

Barford, C. C., Wofsy, S. C., and Goulden, M. L.: Factors controlling long- and short-term sequestration of atmospheric CO_2 in a mid-latitude forest, Science, 294, 1688–1691, 2001.

Behrenfeld, M. J., Randerson, J. T., McClain, C. R., Feldman, G. C., Los, S. O., and Tucker, C. J.: Biospheric primary production during an ENSO transition, Science, 291, 2594–2597, 2001.

Buermann, W., Dong, J., Zeng, X., Myneni, R. B., and Dickinson, R. E.: Evaluation of the

utility of satellite-based vegetation leaf area index data for climate simulations, J. Climate, 14, 3536–3550, 2001.
Chen, B., Chen, J. M., Mo, G., Yuen, C-W., Margolis, H., Higuchi, K., and Chan, D.: Modeling and scaling coupled energy, water, and carbon fluxes based on remote sensing: an application to Canada's landmass, J. Hydrometeorol., 8, 123–143, 2007.
Chen, B., Black, A., Coops, N. C., Hilker, T., Trofymow, T., Nesic, Z., and Morgenstern, K.: Assessing tower flux footprint climatology and scaling between remotely sensed and eddy covariance measurements, Bound.-Lay. Meteorol., 130, 137–167, doi:10.1007/s10546-008-9339-1, 2009a.
Chen, B., Black, A., Coops, N. C., Jassal, R., and Nesic, Z.: Seasonal controls on interannual variability in carbon dioxide exchange of a Pacific Northwest Douglas-fir forest, 1997–2006, Glob. Change Biol., 15, 1962–1981, doi:10.1111/j.1365-2486.2008.01832.x, 2009b.
Chen, J. M., Govind, A., and Sonnentag, O.: Leaf area index measurements at Fluxnet-Canada forest sites, Agr. Forest Meteorol., 140, 257–268, 2006.
Coops, N. C., Black, T. A., Jassal, R. S., Trofymow, J. A., and Morgenstern, K.: Comparison of MODIS, eddy covariance determined and physiologically modelled gross primary production (GPP) in a Douglas-fir forest stand, Remote Sens. Environ., 107, 385–401, 2007.
Cosh, M. H. and Brutsaert, W.: Microscale structural aspects of vegetation density variability, J. Hydrol., 276, 128–136, 2003.
Drolet, G. G., Middleton, E. M., Huemmrich, K. F., Hall, F. G., Amiro, B. D., and Barr, A. G.: Regional mapping of gross light-use efficiency using MODIS spectral indices, Remote Sens. Environ., 112, 3064–3078, 2008.
Falge, E., Baldocchi, D., Olson, R., Anthoni, P., Aubinet, M., Bernhofer, C., Burba, G., Ceulemans, R., Clement, R., Dolmani, H., Granier, A., Gross, P., Gruünwald, T., Hollinger, D., Jensen, N.-O., Katul, G., Keronen, P., Kowalski, A., Lai, C. T., Law, B. E., Meyers, T., Moncrieff, J., Moors, E., Munger, J. W., Pilegaard, K., Rannik, Ü., Rebmann, C., Suyker, A., Tenhunen, J., Tu, K., Verma, S., Vesala, T., Wilson, K., and Wofsy, S.: Gap filling strategies for defensible annual sums of net ecosystem exchange, Agr. Forest Meteorol., 107, 43–69, 2001.
Field, C. B., Randerson, J. T., and Malmstrom, C. M.: Global net primary production-combining ecology and remote sensing, Remote Sens. Environ., 51, 74–88, 1995.
Finnigan, J.: The footprint concept in complex terrain, Agr. Forest Meteorol., 127, 117–129, 2004.

Gobron, N., Pinty, B., Verstraete, M., and Govaerts, Y.: The MERIS Global Vegetation Index (MGVI): description and preliminary application, Int. J. Remote Sens., 20, 1917–1927, 1999.
Gökede, M., Rebmann, C., and Foken, T.: A combination of quality assessment tools for eddy co-variance measurements with footprint modelling for the characterisation of complex sites, Agr. Forest Meteorol., 127, 175–188, 2004.
Govaerts, Y. M., Verstraete, M. M., Pinty, B., and Gobron, N.: Designing optimal spectral indices: a feasibility and proof of concept study, Int. J. Remote Sens., 20, 1853–1873, 1999.
Hall, F. G., Hilker, T., Coops, N. C., Lyapustin, A., Huemmrich, F., Middleton, E., Margolis, H., Drolet, G., and Black, T.: Multi-angle remote sensing of forest light use efficiency by observing PRI variation with canopy shadow fraction, Remote Sens. Environ., 112, 3201–3211, 2008.
Heikkinen, J. E. P., Virtanen, T., Huttunen, J. T., Elsakov, V., and Martikainen, P. J.: Carbon balance in east European tundra, Global Biogeochem. Cy., 18, GB1023, doi:10.1029/2003GB002054, 2004.
Hilker, T., Coops, N. C., Hall, F. G., Black, T. A., Chen, B., Krishnan, P., Wulder, M. A., Sellers, P. J., Middleton, E. M., and Huemmrich, K. F.: A modeling approach for upscaling gross ecosystem production to the landscape scale using remote sensing data, J. Geophys. Res., 113, G03006, doi:10.1029/2007JG000666, 2008.
Huang, M., Ji, J., Li, K., Liu, Y., Yang, F., and Tao, B.: The ecosystem carbon accumulation after conversion of grasslands to pine plantations in subtropical red soil of South China, Tellus, 59B, 439–448, 2007.
Huete, A. R., Liu, H. Q., Batchily, K., and van Leeuwen, W.: A comparison of vegetation indices over a global set of TM images for EOS-MODIS, Remote Sens. Environ., 59, 440–451, 1997.
Huete, A., Didan, K., Miura, T., Rodriguez, E. P., Gao, X., and Ferreira, L. G.: Overview of the radiometric and biophysical performance of the MODIS vegetation indices, Remote Sens. Environ., 83, 195–213, 2002.
Law, B. E., Waring, R. H., and Anthoni, P. M.: Measurements of gross and net ecosystem, productivity and water vapour exchange of a Pinus ponderosa ecosystem, and evaluation of two generalized models, Global Change Biol., 6, 155–168, 2000.
Levy, P. E., Grelle, A., Lindroth, A., Mölder, M., Jarvis, P. G., Kruijt, B., and Moncrieff, J. B.: Regional-scale CO_2 fluxes over central Sweden by a boundary layer budget method, Agr. Forest Meteorol., 98–99, 169–180, 1999.
Li, Z., Yu, G., Xiao, X., Li, Y., Zhao, C., Ren, C., Zhang, L., and Fu, Y.: Modeling gross primary

production of alpine ecosystems in the Tibetan Plateau using MODIS images and climate data, Remote Sens. Environ., 107, 510–519, 2007.
Monteith, J. L.: The photosynthesis and transpiration of crops, Exp. Agr., 2, 1–14, 1966.
Monteith, J. L.: Solar radiation and productivity in tropical ecosystems, J. Appl. Ecol., 9, 747–766, 1972.
Prince, S. D. and Goward, S. N.: Global primary production: a remote sensing approach, J. Biogeogr., 22, 815–835, 1995.
Raich, J. W., Rastetter, E. B., Melillo, J. M., Kicklighter, D. W., Steudler, P. A., Peterson, B. J., Grace, A. L., Moore, B., and Vorosmarty, C. J.: Potential net primary productivity in South-America – application of a global-model, Ecol. Appl., 1, 399–429, 1991.
Ruimy, A., Jarvis, P. G., Baldocchi, D. D., and Saugier, B.: CO_2 fluxes over plant canopies and solar radiation: a review, Adv. Ecol. Res., 26, 1–68, 1995.
Ruimy, A., Kergoat, L., and Bondeau, A.: Comparing global models of terrestrial net primary productivity (NPP): analysis of differences in light absorption and light-use efficiency, Glob. Change Biol., 5, 56–64, 1999.
Running, S. W., Baldocchi, D. D., Turner, D. P., Gower, S. T., Bakwin, P. S., and Hibbard, K. A.: A global terrestrial monitoring network integrating tower fluxes, flask sampling, ecosystem modeling and EOS satellite data, Remote Sens. Environ., 70, 108–127, 1999.
Running, S. W., Nemani, R. R., Heinsch, F. A., Zhao, M., Reeves, M., and Jolly, M.: A continuous satellite-derived measure of global terrestrial primary productivity: future science and applications, Bioscience, 56, 547–560, 2004.
Running, S. W., Thornton, P. E., Nemani, R., and Glassy, J. M.: Global terrestrial gross and net primary productivity from the Earth Observing System, in: Methods in Ecosystem Science, edited by: Sala, O. E., Jackson, R. B., and Mooney, H. A., Springer, New York, 44–57, 2000.
Schmid, H. P.: Experimental design for flux measurements: matching scales of observations and fluxes, Agr. Forest Meteorol., 87, 179–200, 1997.
Shen, S. and Leclerc, M. Y.: How large must surface layer inhomogeneities be before they influence the convective boundary layer structure? A case study, Q. J. Roy. Meteor Soc., 121, 1209–1228, 1995.
Sogachev, A., Rannik, U., and Vesala, T.: Flux footprints over complex terrain covered by heterogeneous forest, Agr. Forest Meteorol., 127, 142–158, 2004.
Stoy, P. C., Katul, G., and Siqueira, G.: Separating the effects of climate and vegetation on evapotranspiration along a successional chronosequence in the southeastern US, Global

Change Biol., 12, 2115–2135, 2006.
Tucker, C. J.: Red and photographic infrared linear combinations for monitoring vegetation, Remote Sens. Environ., 8, 127–150, 1979.
Urbanski, S., Barford, C., and Wofsy, S.: Factors controlling CO_2 exchange on timescales from hourly to decadal at Harvard Forest, J. Geophys. Res., 112, G02020, doi:10.1029/2006JG000293, 2007.
Wen, X., Yu, G., Sun, X., Li, Q., Liu, Y., Zhang, L., Ren, C., Fu, Y., and Li, Z.: Soil moisture effect on the temperature dependence ofecosystem respiration in a subtropical Pinus plantation of southeastern China, Agr. Forest Meteorol., 137, 166–175, 2006.
Xiao, X. M., Zhang, Q. Y., Hollinger, D., Aber, J., and Moore, B.: Modeling gross primary production of an evergreen needleleaf forest using MODIS and climate data, Ecol. Appl., 15, 954–969, 2005.
Xiao, X., Boles, S., Liu, J. Y., Zhuang, D. F., and Liu, M. L.: Characterization of forest types in northeastern China, using multi-temporal SPOT-4 VEGETATION sensor data, Remote Sens. Environ., 82, 335–348, 2002.
Xiao, X., Hollinger, D., Aber, J. D., Goltz, M., Davidson, E., Zhang, Q., and Moore III, B.: Satellite-based modeling of gross primary production in an evergreen needle leaf forest, Remote Sens. Environ., 89, 519–534, 2004.
Zhang, L. M., Yu, G. R., Sun, X. M., Wen, X. F., Ren, C. Y., Fu, Y. L., Li, Q. K., Li, Z. Q., Liu, Y. F., Xin, D., Guan, D. X., and Yan, J. H.: Seasonal variations of ecosystem apparent quantum yield (α) and maximum photosynthesis rate (P_{max}) of different forest ecosystems in China, Agr. Forest Meteorol., 137, 176–187, 2006.

Table 1. Stand characteristics at Qian Yinzhou experiment station in southeastern China*.

Stand species	*Pinus elliottii*	*Pinus massoniana*	*Cunninghamia lanceolata*	Plantation time
Tree height (m)	12.6	10.5	10.8	1983
Diameter at breast height (m)	0.17	0.13	0.14	1983
Tree density (m ha^{-1})	745	880	102	1983

* Data are from a survey made in 2005 (Wen et al., 2006).

BGD
6, 11317–11345, 2009

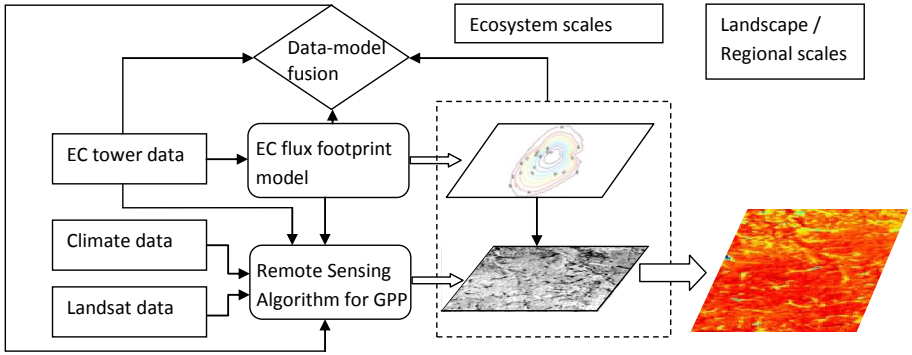

Fig. 1. Flow diagram of the GPP upscaling algorithm based on Landsat and EC tower data.

BGD
6, 11317–11345, 2009

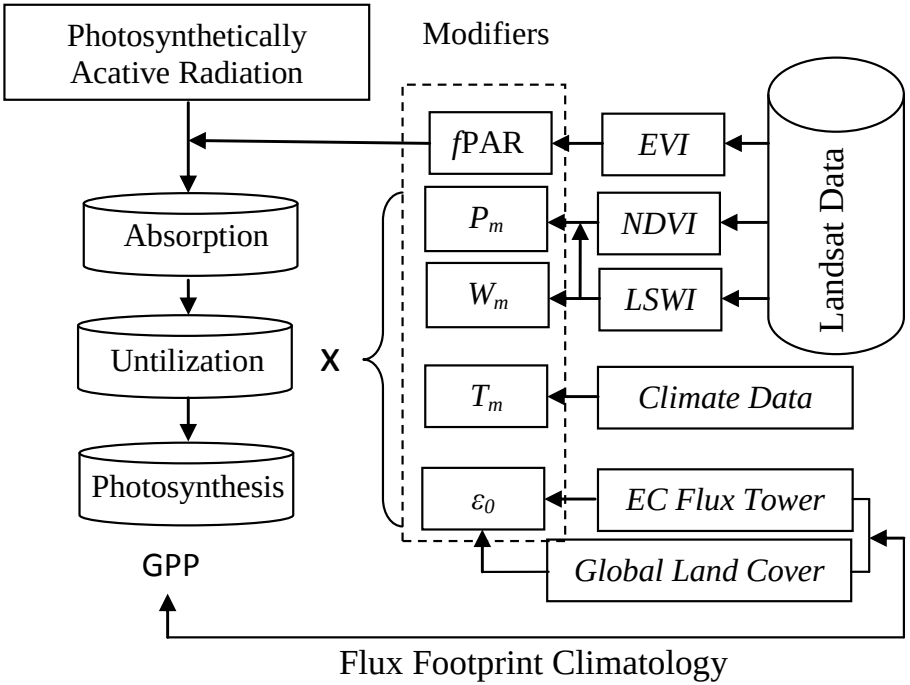

Fig. 2. Flow diagram of the major processing steps of the Landsat-based GPP algorithm. The definitions of symbols and abbreviations are given in text.

BGD
6, 11317–11345, 2009

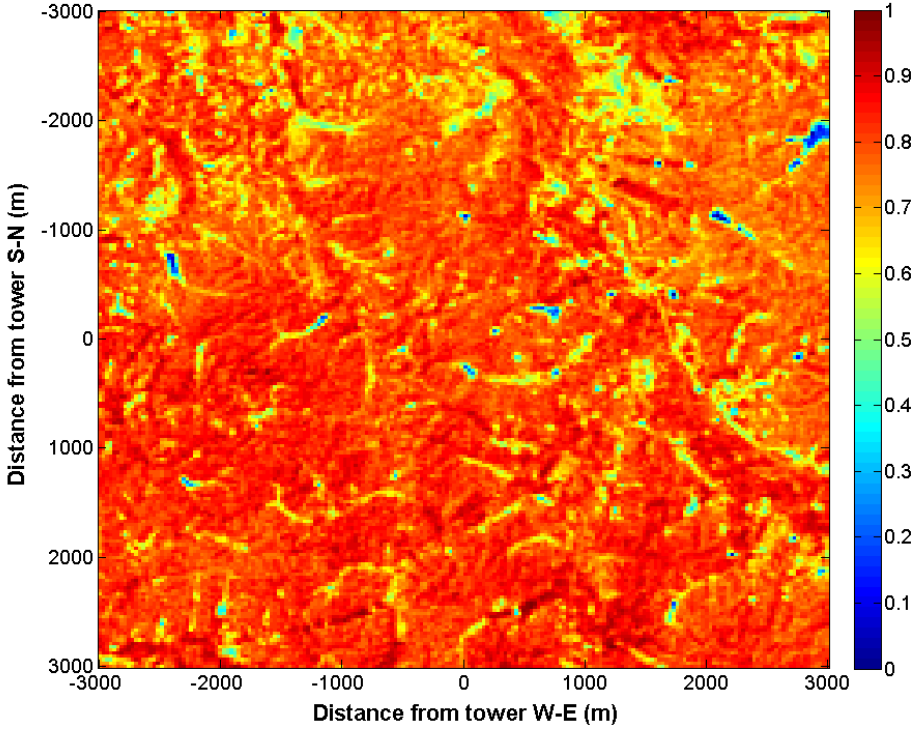

Fig. 3. Land surface heterogeneites of vegetation, indicated by the Normalized Difference Vegetation Index (NDVI), for the area (domain) of 6 km×6 km centered at the Qian Yinzhou flux tower in an evergreen needleleaf forest, China. The NDVI was calculated from a Landsat scene on 3 October 2004.

BGD
6, 11317–11345, 2009

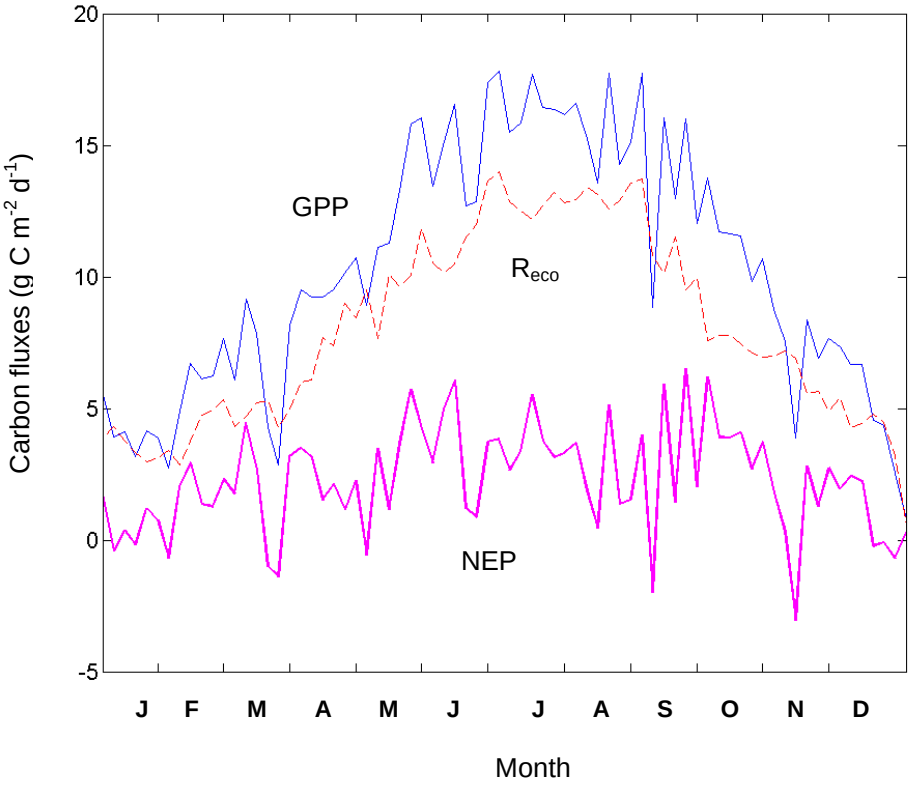

Fig. 4. Five-day ensemble means of CO_2 component fluxes for the year of 2004 measured at the Qian Yinzhou flux tower in an evergreen needleleaf forest, China. Measured net ecosystem productivity (NEP) was partitioned into gross primary productivity (GPP) and ecosystem respiration (R_{eco}) using procedures described in Wen et al. (2006).

BGD
6, 11317–11345, 2009

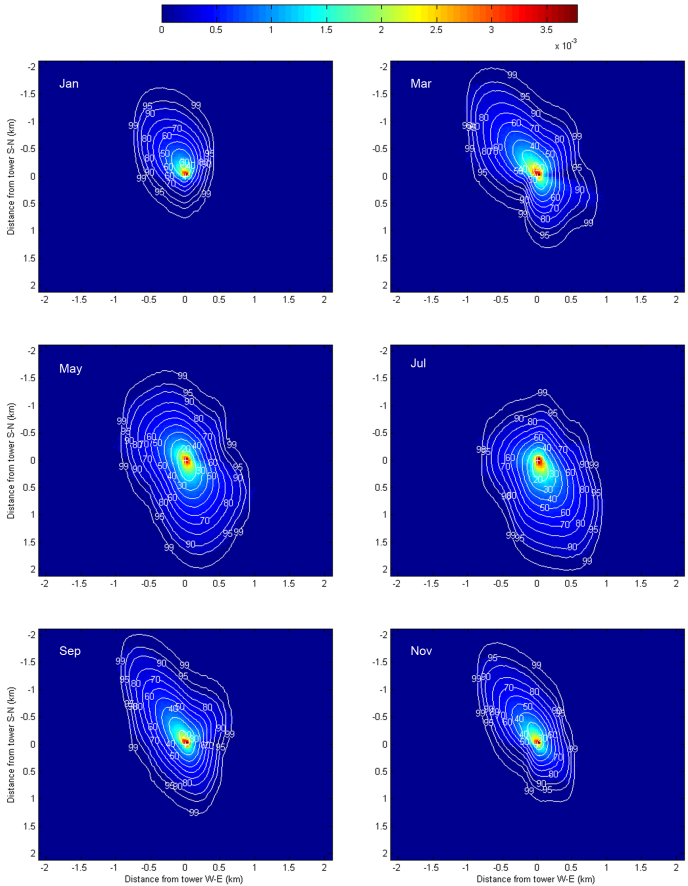

Fig. 5. Mean monthly daytime pure footprints and the corresponding cumulative footprint contours for every other month in 2004 for the Qian Yinzhou flux tower in an evergreen needleleaf forest, China.

BGD

6, 11317–11345, 2009

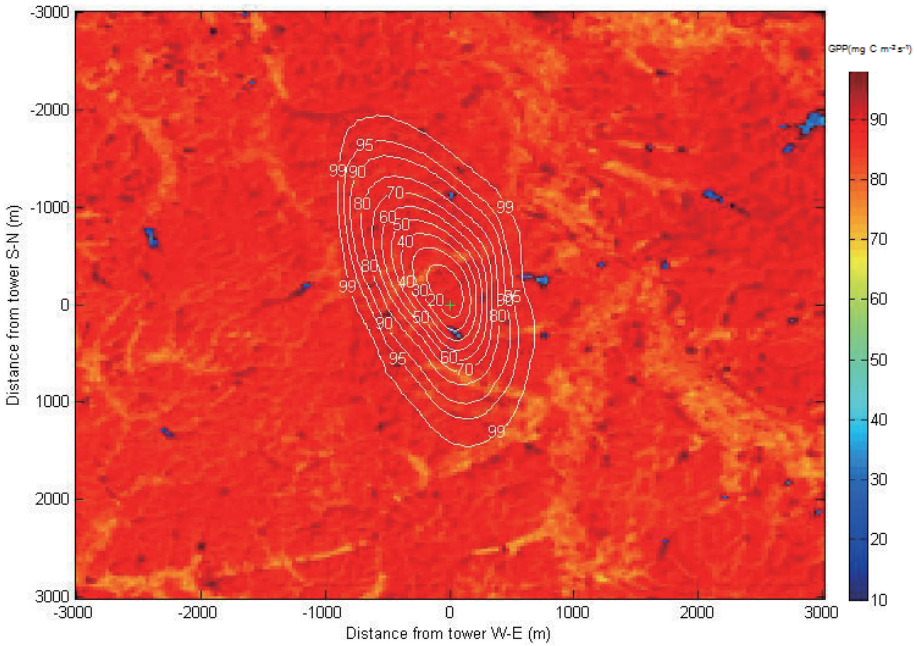

Fig. 6. Remotely-sensed annual mean gross primary (GPP) map at 30-m resolutions surrounding the QYZ tower for 2004, overlaid by corresponding cumulative annual mean daytime pure (unweighted) footprint climatology contours.

BGD
6, 11317–11345, 2009

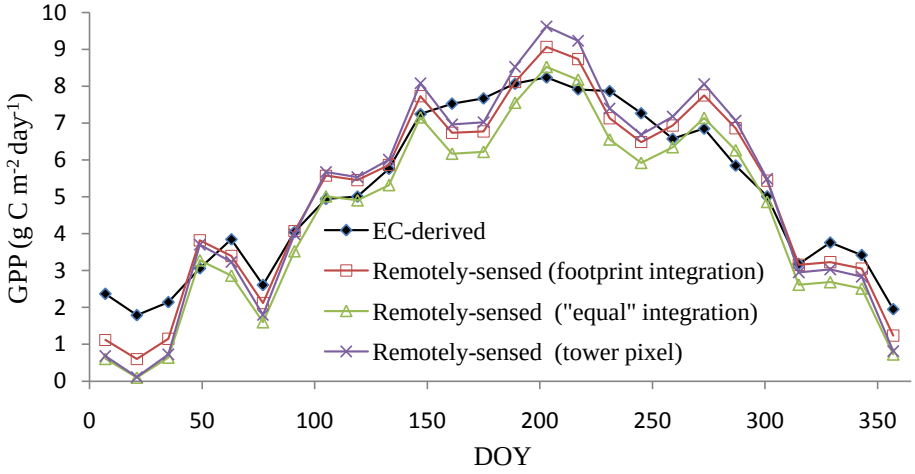

Fig. 7. A comparison of the seasonal dynamics between the observed gross primary production (GPP) and remotely sensed GPP in 2004 in an evergreen needleleaf forest at QYZ, China.

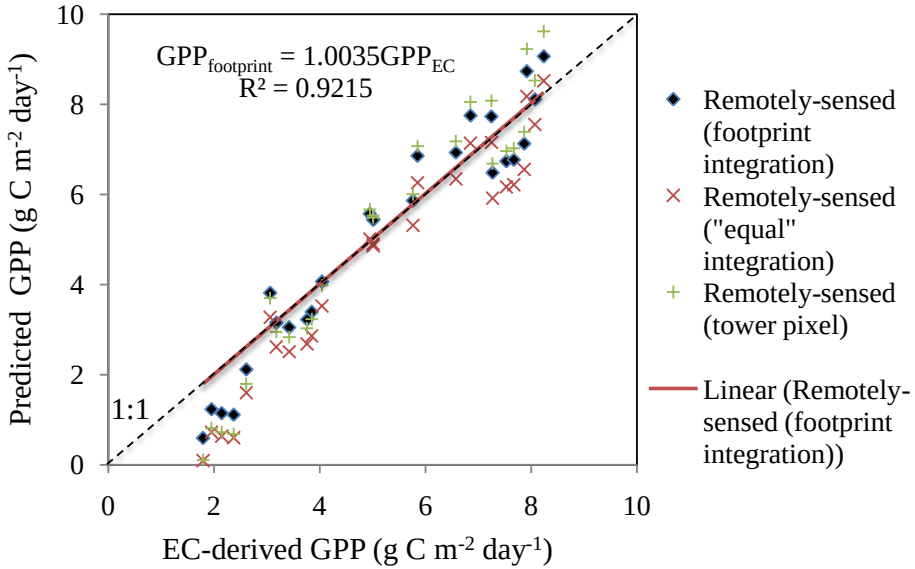

Fig. 8. A comparison of biweekly gross primary production (GPP) values between the observed (EC-derived) and predicted (remotely sensed) in 2004 in an evergreen needleleaf forest at QYZ, China.

BGD
6, 11317–11345, 2009